Deep sea cold seeps are a sink for mercury and source for methylmercury

Jiwei Li, Xiyang Dong, Yongjie Tang, Chuwen Zhang, Yali Yang, Wei Zhang, Shanshan Liu, Wei Yuan, Xinbin Feng, Lars-Eric Heimbürger-Boavida, et al.

communications earth & environment

Article

https://doi.org/10.1038/s43247-024-01484-7

Deep sea cold seeps are a sink for mercury and source for methylmercury

Jiwei Li[1,8], Xiyang Dong[2,8], Yongjie Tang[1], Chuwen Zhang[2], Yali Yang[1], Wei Zhang[3], Shanshan Liu[4], Wei Yuan[3], Xinbin Feng[3,5], Lars-Eric Heimbürger-Boavida[6], Feiyue Wang[7], Lihai Shang[3] ✉ & Xiaotong Peng[1] ✉

The effect of seafloor cold seeps on the biogeochemical cycling of mercury (Hg) remains enigmatic. Here we demonstrate substantial enrichments of mercury and methylmercury, along with the presence of microbes capable of metabolizing mercury in sediments of the Haima cold seep, South China Sea, by analyzing mercury and methylmercury concentrations, mercury isotopic composition analyses and metagenomic analyses of sediment cores. Compared to the reference area, the sediments in the upper sediment column of the active-seep area were 2.4 times enriched in Hg and 10.5 times in methylmercury. The slope of the capital delta ratio of mercury 199 to mercury 201 ($\Delta^{199}Hg/\Delta^{201}Hg$) with 1.23 ± 0.10 in the active-seep area indicate the occurrence of dark redox reactions. Genes related to mercury methylation (*hgcA*), demethylation (*merB*) and reduction (*merA*) were phylogenetically associated with several bacterial and archaeal linages. We roughly estimated an additional 2,835 Mg mercury and 9 Mg methylmercury are stored in cold seep globally. In summary, we propose that cold seeps globally function as a previously unrecognized sink for mercury and source for methylmercury in the deep ocean.

Mercury (Hg) is a metal of environmental concern, with most natural and anthropogenic inputs occurring in its inorganic form[1]. In aquatic ecosystems, inorganic Hg can be transformed into methylmercury (MMHg), which is a bioaccumulative and biomagnifying neurotoxin and can pose a potent threat to human and ecosystem health globally[2,3]. The ocean plays an important role in global Hg cycling[4–7], as it receives Hg from various pathways such as atmospheric deposition, gas invasion, riverine and submarine groundwater discharge, and hydrothermal venting[8–10]. MMHg has been found to be enriched in the subsurface ocean[10–14], which represents a major exposure pathway for humans via the consumption of fish and marine mammals foraging at these depths (100–1000 m). However, it is uncertain whether the deep ocean has the capacity for Hg methylation and demethylation[13].

Seafloor cold seeps occur in a variety of geological settings along tectonic plate margins[15,16]. In cold seep environments, microbial sulfate reduction, anaerobic methane oxidation, and methanogenesis are known to occur, supporting a diverse community of chemosynthetic organisms[17–19]. As sulfate-reducing bacteria, methanogens, and anaerobic methane-oxidizing archaea are known Hg methylators[3,20], seafloor cold seeps could be globally important hotspots for Hg(II) methylation and/or MMHg demethylation, which have not been accounted for in global Hg models.

To test this hypothesis, here we investigated Hg and MMHg concentrations, Hg isotopic composition, and metagenomic analyses for 5 sediment cores (A2, A3, A4, B1, B2, and C1) and two species of bivalves (a mussel (*Gigantidas haimaensis*) and a vesicomyid clam *(Calyptogena marissinica)*) collected from three different environments of the Haima cold seep, South China Sea (Supplementary Fig. 1). Cores A2, A3, and A4 were collected from a reference area around the cold seep, Cores B1 and B2 from an active methane seep area densely covered with living *G. haimaensis*, and core C1 from an inactive methane seep area covered with *C. marissinica* with both living and dead clams.

Results and discussion

Enrichment of Hg and MMHg in cold seep environments

In this study, Hg concentrations are significantly higher in the upper sediment column (0–12 cm) from the active area than those in the inactive area ($p < 0.01$) and reference site ($p < 0.001$). The average concentrations of Hg in sediments above 12 cm from the active seep area

[1]Institute of Deep-Sea Science and Engineering, Chinese Academy of Sciences, Sanya, China. [2]Key Laboratory of Marine Genetic Resources, Third Institute of Oceanography, Ministry of Natural Resources, Xiamen, China. [3]State Key Laboratory of Environmental Geochemistry, Institute of Geochemistry, Chinese Academy of Sciences, Guiyang, China. [4]BGI-Qingdao, Qingdao, China. [5]University of Chinese Academy of Sciences, Beijing, China. [6]Aix Marseille Université, CNRS/INSU, Université de Toulon, IRD, Mediterranean Institute of Oceanography (MIO), Marseille, France. [7]Centre for Earth Observation Science, Department of Environment and Geography, University of Manitoba, Winnipeg, MB, Canada. [8]These authors contributed equally: Jiwei Li, Xiyang Dong.
✉e-mail: shanglihai@vip.skleg.cn; xtpeng@idsse.ac.cnm

(97.2 ± 37.2 ng g^{-1}, $n = 10$) are 2.3 and 2.4 times higher than those of inactive seep area (42.8 ± 4.18 ng g^{-1}, $n = 6$) and the reference site (40.4 ± 6.49 ng g^{-1}, $n = 14$) (Supplementary Fig. 2 and Supplementary Data 1), respectively. In contrast, sediment samples below 12 cm from the active seep area (38.7 ± 5.88 ng g^{-1}, $n = 12$) have similar Hg levels to the inactive seep area (33.5 ± 6.00 ng g^{-1}, n = 16) and reference area (41.1 ± 0.91 ng g^{-1}, $n = 5$). Our reference site corresponds well with the deep basin sediment Hg concentrations (38.0 ± 21.0 ng g^{-1}) in the Atlantic Ocean[21]. The concentration of Hg in the core-top layer (0–2 cm) of the active seep area is three times higher (164 ng g^{-1}) than those of the reference area (51.1 ng g^{-1}) (Fig. 1 and Supplementary Data 1). This value is also much higher than those of recently reported Hg-rich Mariana hadal trench zone[5] (89.0 ± 33.0 ng g^{-1}, top ~10 cm) but lower than maximum concentrations in Atacama trench (up to 400 ng g^{-1}, top 2 cm)[22]. Consistent with the sediment results, the tissues of *G. haimaensis* living in the active seep area also contained higher total Hg (gill, 280 ng g^{-1}; mantle, 90.7 ng g^{-1}) compared to *C. marissinica* (gill, 68.3 ng g^{-1}; mantle, 41.5 ng g^{-1}) living in the inactive seep area (Supplementary Data 1). This phenomenon is comparable to mussel samples from the Site F cold seep in the South China Sea. Yuan et al. reported that the bathymodiolin mussel *Bathymodiolus aduloides* (592–920 ng g^{-1}) living in the center of the cold seep had a much higher Hg concentration than those of *Gigantidas platifrons* (46.0–173 ng g^{-1}) living more distant[23].

Sediment organic matter is an important factor controlling Hg distribution and speciation in marine sediments[22,24–26]. Reduced sulfur moieties in the natural organic matter can bind Hg[27,28]. Correspondingly, the observed total Hg was significantly correlated with total organic carbon content (TOC) in all sediment cores ($R^2 = 0.39$, $p < 0.05$, Supplementary Fig. 3). Hg/TOC is commonly used as an indicator to measure the ability of TOC to sorb Hg[22,25]. The value of Hg/TOC in sediments of the active seep area is enriched when compared to the inactive seep area and reference area (Fig. 1). This suggests that the ability of TOC to sorb Hg in the active seep area is, on average, higher than that of background marine sediments, or organic carbon that do not bind strongly to mercury are preferentially degraded.

MMHg concentrations (Supplementary Fig. 2 and Supplementary Data 1) in the upper sediment column (0–12 cm) from the seep areas (active: 0.21 ± 0.37 ng g^{-1}, $n = 5$; inactive: 0.21 ± 0.36 ng g^{-1}, $n = 6$) were, on average, higher than those of the reference area (0.02 ± 0.01 ng g^{-1}, $n = 6$). We observed the MMHg and MMHg/Hg maxima co-occurred in sediment

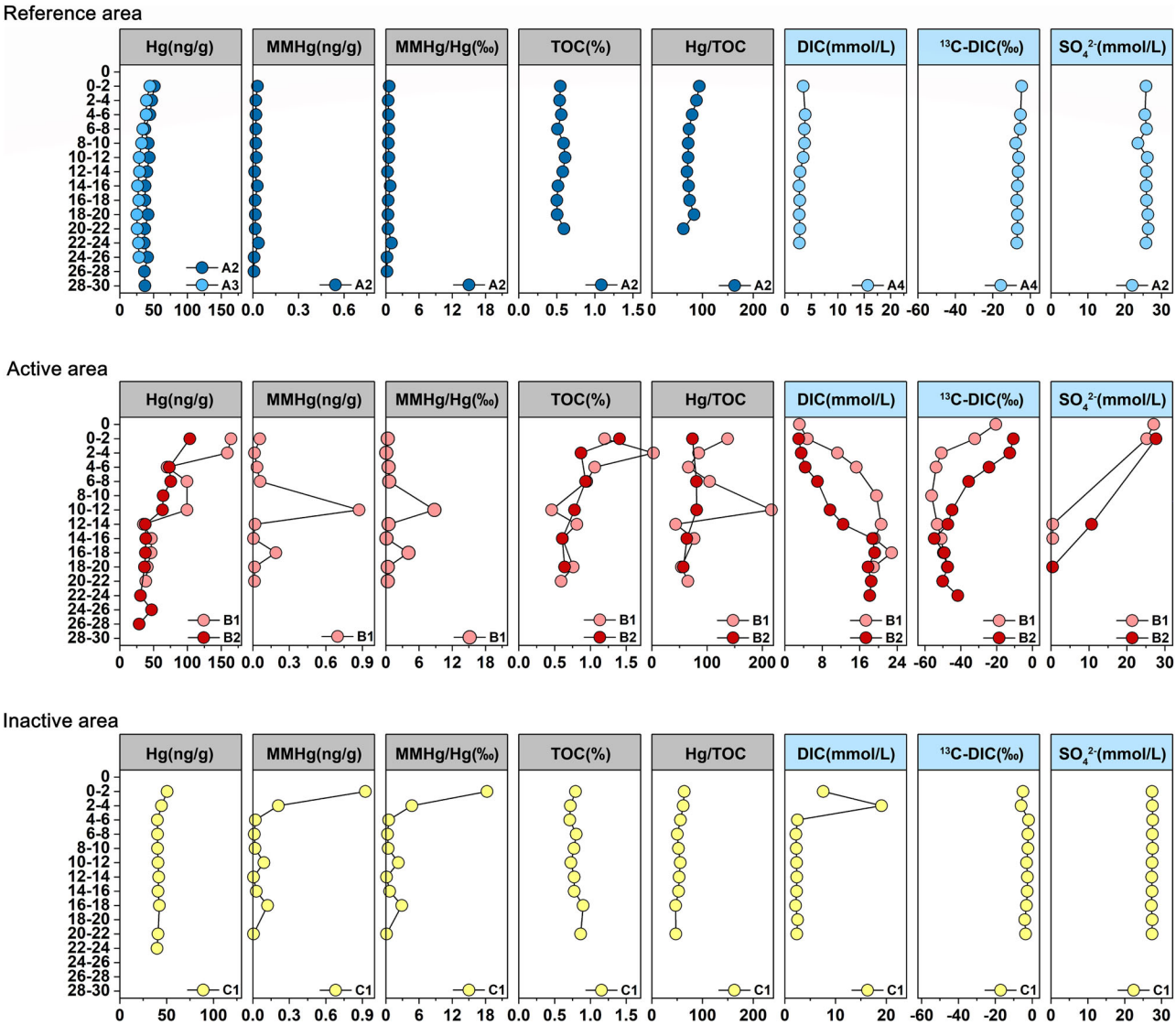

Fig. 1 | The depth profile of the geochemical characteristics in the sediment cores from the Haima cold seep, South China Sea. Hg, MMHg, MMHg/Hg, TOC, and Hg/TOC in the sediments, and DIC, δ^{13}C-DIC, and SO_4^{2} in the pore water of the sediment cores (A2–+A4) from the reference area, the active seep area (B1 and B2), and the inactive seep area (C1) of the Haima cold seep, South China Sea.

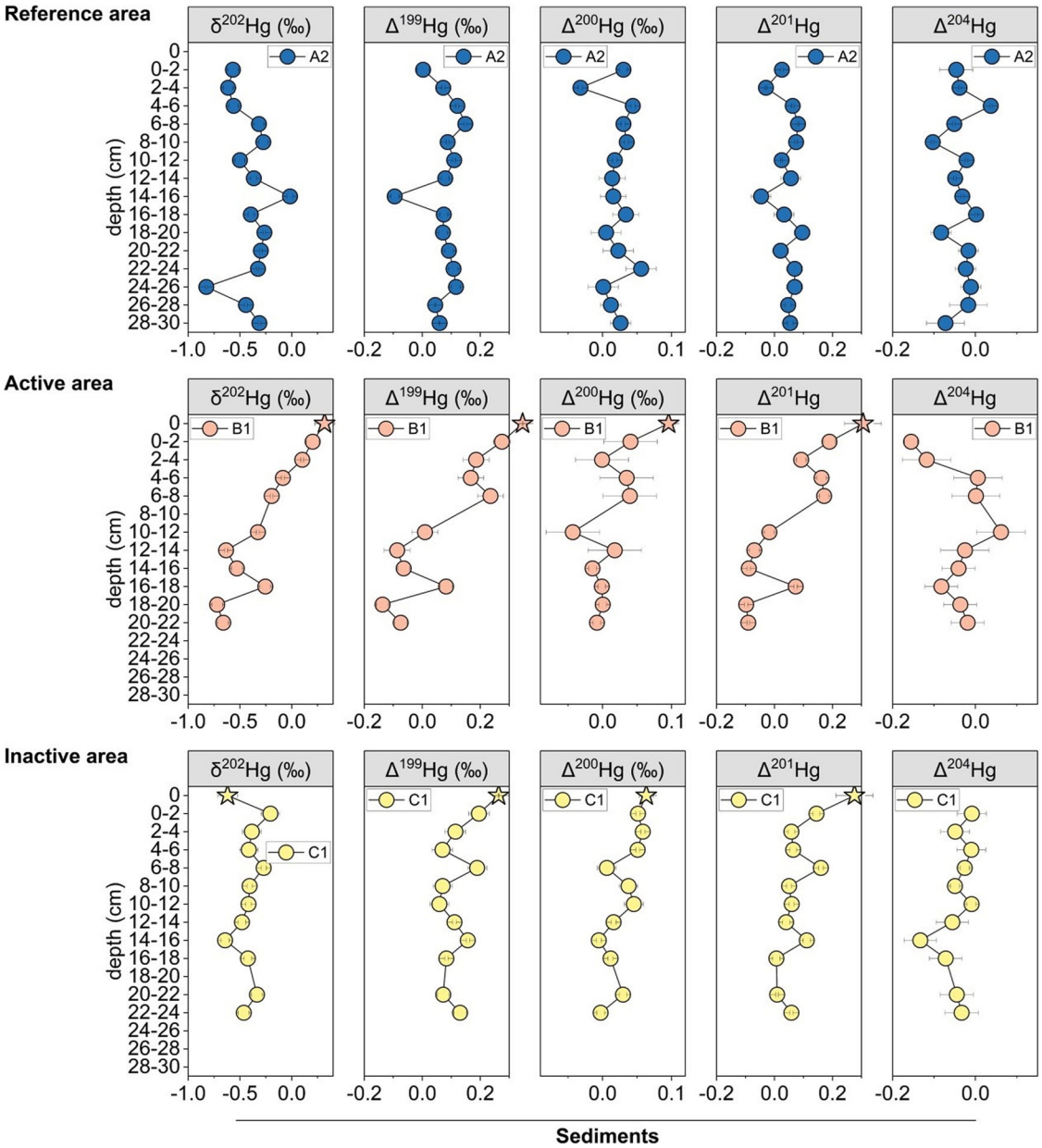

Fig. 2 | The depth profile of Hg isotopes in the sediment cores from the Haima cold seep, South China Sea. $\delta^{202}Hg$, $\Delta^{199}Hg$, $\Delta^{200}Hg$, $\Delta^{201}Hg$, and $\Delta^{204}Hg$ values in the sediment cores from the reference area (A2), the active seep area (B1), and the inactive seep area (C1) of the Haima cold seep, South China Sea. The error bars on individual samples represent 2 SD analytical uncertainty.

cores of both active and inactive seep areas (Fig. 1 and Supplementary Data 1). The value of MMHg/Hg maxima is about 8 and 18 times higher, respectively than those of the reference area. In the active seep area, the MMHg maximum also coincided with the depth of Hg/TOC maximum and appeared within the sulfate methane transition zone (SMTZ) of this site[16], where low sulfate concentrations (0.47–0.49 mM) and depleted $\delta^{13}C_{DIC}$ values (up to −56.31‰) were observed. This may be because the dynamic microbial sulfate reduction and anaerobic methanotrophic activities in the SMTZ create conditions conducive to the activity of known Hg methylators[29,30]. In the inactive seep area (Fig. 1 and Supplementary Data 1), however, the MMHg and MMHg/Hg both peaked at the core-top layer, where strong organic matter decomposition activities were found as evidenced by extremely high content of dissolved inorganic carbon (DIC, 19.1 mM) and values of $\delta^{13}C$-DIC (−5.95‰) are much higher than those found in the surface sediment of the active area and similar to those of the reference area. This result is consistent with the observation of many dead clams (*C. marissinica*) in this area (Supplementary Fig. 1d). The degradation of clam tissues would also lead to the increase of pore water DIC content[31], which is possibly an additional driver of Hg methylation as it influences both Hg bioavailability and microbial activities[32]. In addition, consistent with Yuan et al.[23], the methylmercury content of bivalves was extremely low: below detection limits (0.002 ng g^{-1}) and less than 1% of total mercury. This may be related to shorter food chains resulting in a less pronounced biomagnification effect in hydrothermal fields and cold seep environments.

Mercury isotope fractionation in cold seep environments

Hg-stable isotopes are now widely used to trace the sources and processes of Hg in the environment[13]. Distinct mass-dependent fractionation of Hg isotopes (MDF, $\delta^{202}Hg$) and mass-independent fractionation of odd-mass number Hg isotopes (odd-MIF, $\Delta^{199}Hg$, and $\Delta^{201}Hg$) occur during Hg biogeochemical cycling[33,34].

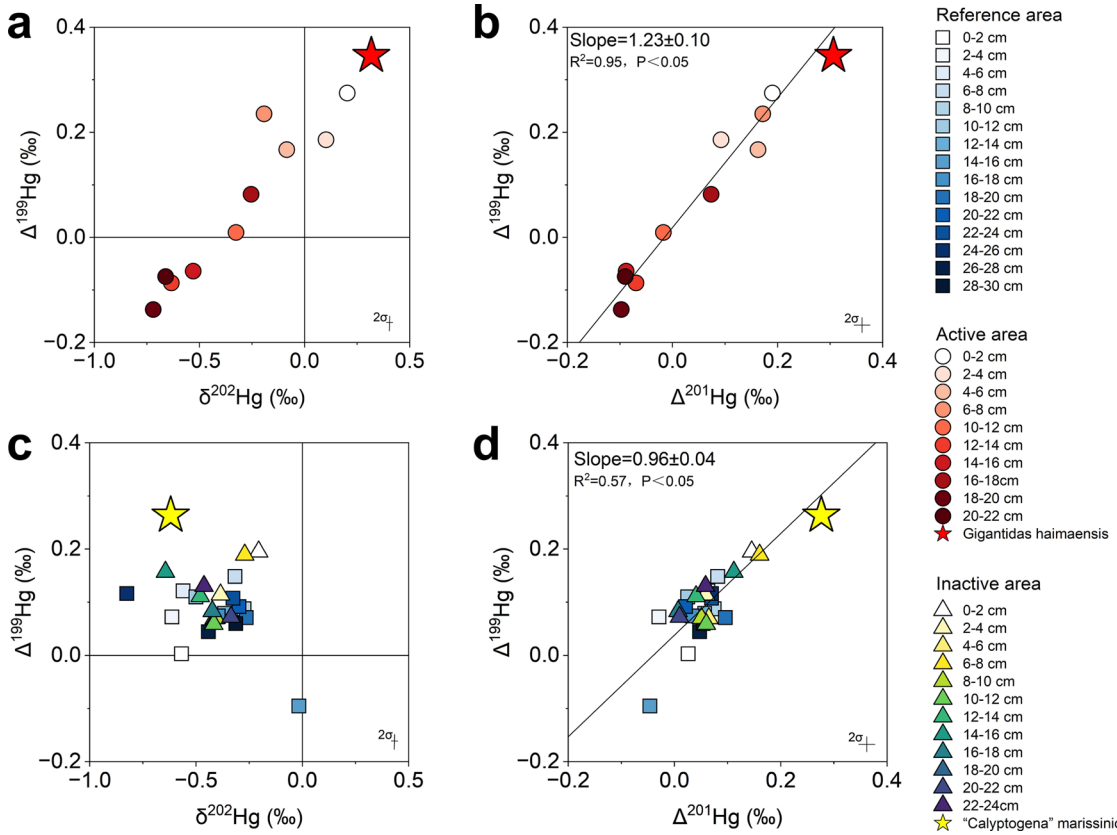

Fig. 3 | Plots of Hg isotopes in the sediment cores and mussels from the Haima cold seep, South China Sea. a Δ^{199}Hg versus δ^{202}Hg values in the sediments of the active seep area. **b** Δ^{199}Hg versus Δ^{201}Hg values in the sediments of the active seep area. **c** Δ^{199}Hg versus δ^{202}Hg values in the sediments of the reference and inactive seep areas. **d** Δ^{199}Hg versus Δ^{201}Hg values in the sediments of the reference area and inactive seep area. The yellow star represents the *C. marissinica* from the inactive seep area, and the red star represents the *G. haimaensis* from the active seep area.

Our results show that Hg isotopic compositions for both MDF and MIF in the active seep area are different from those in the inactive seep area and reference site and those typical of the upper ocean (Figs. 2 and 3 and Supplementary Data 1).

In this study, δ^{202}Hg in *G. haimaensis* has a positive value of 0.32‰, which is comparable to the core-top sediment in the active seep area with 0.20‰. In contrast, δ^{202}Hg in *C. marissinica* living in the inactive seep area shows a distinct negative value with −0.62‰, which is much lower than biota in the active seep area but is comparable to those of mussel samples from the Site F cold seep (−0.74‰ to −0.42‰)[23]. Notably, δ^{202}Hg in the sediment core of the active seep area shows an evidently decreasing pattern from 0.20‰ to −0.72‰ with depth (Fig. 2), while their values in the reference site (0.02‰ to −0.83‰) and inactive seep area (−0.21‰ to −0.64‰) are variable but have no depth trend in the vertical profile. Positive odd Hg-MIF values were observed in most of these sediments and biota samples (Figs. 2 and 3, and Supplementary Data 1). The Δ^{199}Hg has a value of 0.35‰ in *G. haimaensis*, and 0.26‰ in *C. marissinica*, respectively. The Δ^{199}Hg has average values of 0.07‰ ± 0.06‰ ($n = 15$) in the reference site, and 0.11‰ ± 0.05‰ in the inactive site ($n = 11$), respectively. Although in the active site, the Δ^{199}Hg have average values of 0.06‰ ± 0.15‰ ($n = 10$), respectively, the two cores (B1 and B2) both have an evident decrease trend with depth (from 0.27‰ to −0.14‰ of Δ^{199}Hg).

It has been reported that Hg odd-MIF mainly accompanies photoreduction of Hg(II) or photodegradation of MMHg in the aqueous environment[10,35]. The Δ^{199}Hg/Δ^{201}Hg ratio is diagnostic of these two pathways, with a ratio of 1.3 for MMHg photodegradation and 1.0 for Hg(II) photoreduction[35]. In this study, Δ^{199}Hg and Δ^{201}Hg values of sediments in the inactive seep area and reference area are significantly correlated ($R^2 = 0.95$, $p < 0.05$) with a Δ^{199}Hg/Δ^{201}Hg slope of 0.96 ± 0.04 (Fig. 3). This result indicates that part of Hg in the inactive seep area and reference area might have experienced a photoreduction process before settling down into the dark zone of the deep ocean. This conclusion is also supported by the near-zero Δ^{200}Hg values in this whole region (with average values of 0.01‰ ± 0.03‰, 0.03‰ ± 0.02‰ and 0.02‰ ± 0.02‰ in the active site, inactive site and reference site, respectively; Supplementary Data 1), which were similar with sediment samples taken from hadal trench zone[5] and Mediterranean Sea[36]. Notably, an interesting finding is that the slope of Δ^{199}Hg/Δ^{201}Hg in the sediments of the active seep area is 1.23 ± 0.10, which significantly differs from those of the reference and inactive seep areas. Given that the location of the active seep area is very close to the reference and inactive seep area, the Hg deposition from the top sea should be comparable among the above three areas. It is speculated that the distinctive slope of Δ^{199}Hg/Δ^{201}Hg with 1.23 ± 0.10 is induced by some characteristic processes that occurred at an active cold seep system. Zheng and coauthors[37,38] reported that abiotic dark redox reactions of Hg would lead to negative MIF owing to nuclear volume effects, with a linear slope of 1.28 (oxidation) and 1.60 (reduction) for Δ^{199}Hg/Δ^{201}Hg ratios. Therefore, we propose that the Hg deposition process in active seep areas might be also influenced by abiotic dark redox processes. The presence of large amounts of organic matter in the active cold seep may stimulate dark redox processes.

As mentioned above, both of MDF and MIF have an evident decrease trend with depth, while they remain relatively constant in the inactive seep area and reference area. In the sediment cores of the active seep area, the upper sediments have a pronounced positive MDF (δ^{202}Hg up to 0.20‰) and odd-MIF when compared to those of lower parts (Fig. 2 and Supplementary Data 1). Among many possible scenarios for this, two of them are provided here. Firstly, inorganic Hg from the upper ocean transfers into the seep area, where abundant reduced sulfur moieties from seep ecosystems

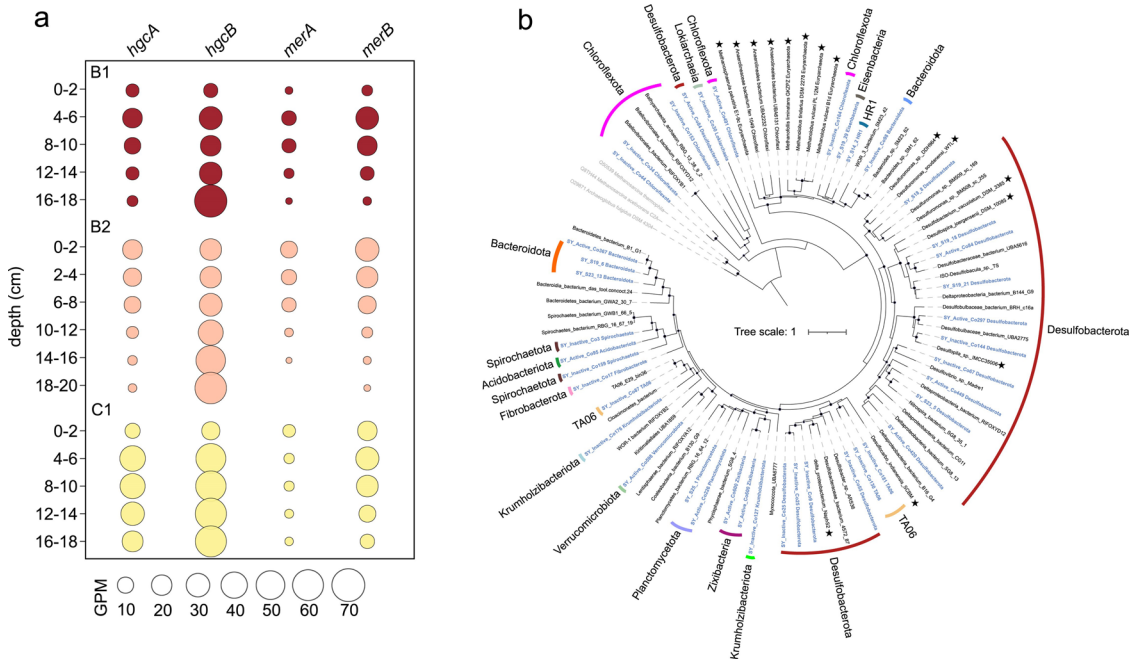

Fig. 4 | The microbially-driven Hg metabolism in the Haima cold seep sediments. **a** The abundances of the Hg-metabolizing genes for different depths in three cores are shown as GPM (Genes Per Million). B1 and B2 were collected from the active area, and C1 was collected from the inactive area. Detailed information on gene abundances is presented in Supplementary Data 4. **b** Maximum-likelihood phylogenetic tree of HgcA amino acid sequences. HgcA sequences recovered in this study are highlighted in blue. HgcA sequences retrieved from public databases are shown in black. Experimentally confirmed HgcA from previous studies are indicated with stars. Bootstrap values of >70% are indicated as black circles at the nodes, and the scale bar indicates substitutions per site.

provide binding sites[27,28], facilitating the Hg deposition and enrichment here. Thus, Hg deposited through this process can inherit the isotopic fingerprint of the Hg in the upper ocean, resulting in a positive odd-MIF but slightly negative MDF [10,13,36]. Secondly, a large amount of Hg^0 rising from the deep would be oxidized to Hg(II) through dark reactions in the absence of light slightly below the sediment-water interface. This process can cause the produced Hg(II) to exhibit a distinct positive MDF [38,39]. Considering these two processes collectively, the surface sediments in the active seep area exhibit significant enrichment of total-Hg concentration and show evident positive MDF and odd-MIF characteristics.

Furthermore, the lower part sediments in the active seep area gradually shift towards negative MDF and odd-MIF characteristics. These features could be attributed to the occurrence of secondary processes, such as abiotic dark reduction and adsorption of Hg, in the sediment columns after Hg deposition. In the active seep area, the lower section of the sediment core is primarily under anoxic conditions. In this environment, the organic matter-driven dark reduction of Hg converts sediment Hg(II) into Hg°, leading to a notable negative odd-MIF in the remaining Hg(II)[38]. In addition, it has been reported that processes such as adsorption by sulfhydryl and Fe groups can retain the lighter fraction of MDF in the residual Hg fraction[40]. Therefore, as time goes on, the deep sediments exhibit negative shifts in both MDF and odd-MIF, which has also been observed in iron-rich soil profiles[40]. In addition, such a reduction would cause a decrease in Hg concentrations.

Evidence for microbially mediated Hg cycling in the cold seep environments

To identify potential microbially-mediated Hg transformations within the cold seep environments, we performed metagenomic sequencing of microbial community DNA extracted from sediment samples of the active-area (B1 and B2) and inactive-area (C1). Results showed that Hg-related functional genes, encoding the capability for Hg methylation (*hgcA*), reduction (*merA*) and demethylation (*merB*) were abundant in cold seep sediments based on gene-revolved analysis (Fig. 4a and Supplementary Data 2). For the inactive seep core C1 and active core B1, the abundance of *hgcA* gene increased with depth, both peaking at 4–6 cm below the sediment-water interface (37 genes per million; GPM) in core C1; 18 GPM in core B2). In the active core B2 samples, *hgcA* gene abundance showed a maximum at the surface sediments (0–2 cm depth, 18 GPM) and decreased with depth. The vertical distribution of the abundance was similar for the *merB* gene and *hgcA* gene. This result suggests the co-occurrence of methylators and de-methylators regulating the apparent MMHg levels. The *merA* gene was observed in low abundance in all cold seep samples.

We conducted metagenomic binning to examine the dominant Hg-metabolizing microbiota in seep sedimentary environments. A total of 487 metagenome-assembled genomes (MAGs) were recovered from all cold-seep metagenomic datasets (Supplementary Data 3). From these, 38 MAGs were identified as putative Hg methylators encoding the *hgcA* genes. They belong to 14 diverse phyla: Desulfobacterota, Zixibacteria, Verrucomicrobiota, TA06, Spirochaetota, Planctomycetota, Krumholzibacteriota, Fibrobacterota, Eisenbacteria, Chloroflexota, Bacteroidota, Acidobacteriota, Halobacteriota and Asgardarchaeota (class of Lokiarchaeia) (Fig. 4b). Among these, Zixibacteria, TA06, Krumholzibacteriota, Eisenbacteria and Lokiarchaeia have not been implicated in Hg methylation. These five newly identified clades were rare (0.04% of the microbial communities on average) in all cold seep samples (Supplementary Data 4). Thirteen *hgcA*-carrying MAGs were associated with Desulfobacterota, representing the most diverse Hg-methylating clade currently known[41]. Desulfobacterota were identified as the dominant Hg-methylator in the upper zone of three sediment cores; their abundance decreased with the sediment depth (Supplementary Fig. 4). Five *hgcA*-carrying MAGs represented members of Chloroflexota, a widespread and dominant clade in most marine sediments[42]. Chloroflexota were observed to be more abundant in the inactive cores than in active cores. One MAG affiliated with HR1 (i.e., ANME-2) within Halobacteriota represented the most abundant archaeal Hg methylators (up to 2.9% of the microbial communities in core C1). The abundance of HR1 showed an increasing trend with depth.

Microbes have been shown to respond to MMHg stress[43] by using the organomercurial lyase encoded by the *merB* gene to demethylate MMHg into Hg^{2+}. In this study, six MAGs, assigned to Chloroflexota, Planctomycetota, and Gammaproteobacteria, were observed to harbor the *merB* gene

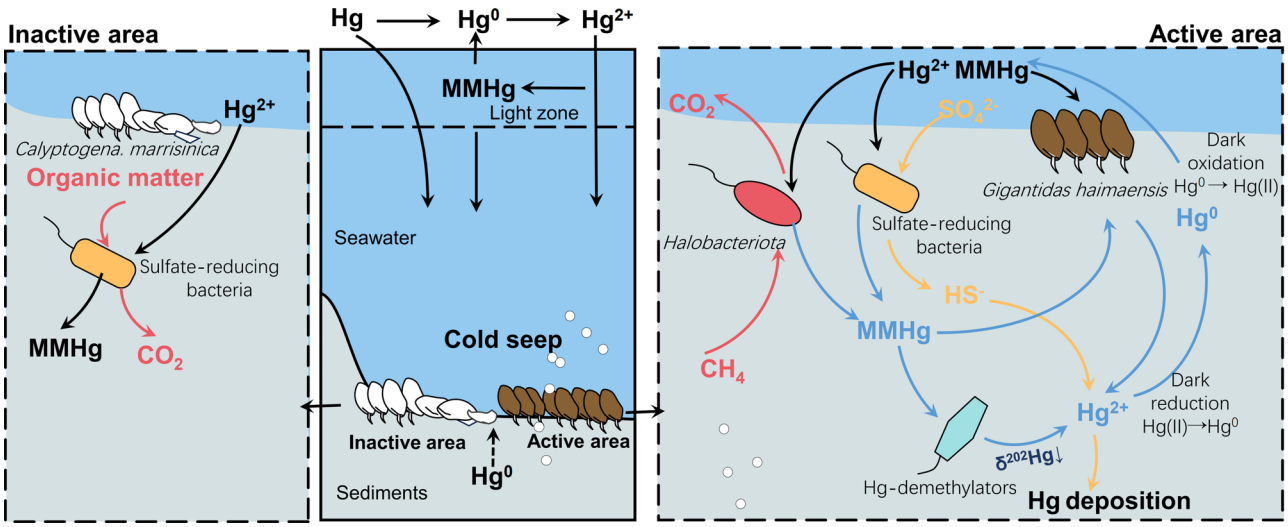

Fig. 5 | The schematic model for the biogeochemical Hg cycle in the seep environment. The cold seep environment continuously receives inorganic Hg deposited from the surrounding environments as the thriving seep ecosystem supplies a large amount of organic matter, which can provide binding sites for Hg absorptions. Part of inorganic Hg(II) is converted into MMHg by Hg-methylators, and microbially-mediated demethylation processes of MMHg also occur. Hg^0 rising from the deep would be oxidized to Hg(II) in the upper oxidized environment, while organic matter-driven abiotic dark reduction converts sediment Hg(II) into Hg°.

(Supplementary Fig. 4 and Supplementary Data 4). Among them, Planctomycetota and Gammaproteobacteria were present in all three sediment cores, while Chloroflexota only occurred in the inactive seep area. Meanwhile, the relative abundance of Proteobacteria and Chloroflexota decreased with sediment depth, while Planctomycetota increased with depth. Additionally, microbes have been shown to cope with Hg^{2+} toxicity by transforming it into volatile Hg^0 using mercuric reductase encoded by the *merA* gene[43]. One MAG belonging to Gammaproteobacteria was found to harbor the *merA* gene.

A schematic model for the biogeochemical Hg cycle in the seep environment and implications

Based on the above geochemical and microbial evidence in the Haima cold seep, we propose a schematic model for the biogeochemical Hg cycle in the cold seep environment (Fig. 5). The thriving seep ecosystem (e.g., *G. haimaensis*) supplies a large amount of thiol compounds and organic matter in the sediments of the active seep area, which can provide binding sites for Hg. Consequently, Hg deposited from surrounding environments would continue to be accumulated here. Within the surface sedimentary environments, part of inorganic Hg(II) is converted into MMHg by Hg-methylators, such as sulfate-reducing bacteria and methanotrophic microorganisms. Microbial mediated-demethylation processes of MMHg might also occur, indicated by the presence of members of Chloroflexota, Planctomycetota and Gammaproteobacteria. The rate and efficiency of microbial methylation and demethylation processes would peak under certain conditions due to diagenesis and microbial activities in the sediment core. As indicated by the Hg odd-MIF values in the active seep area, a large amount of thiol compounds and organic matter creates an ideal condition for the occurrence of abiotic dark redox transformation of Hg. In the upper oxidized environment, as Hg^0 undergoes oxidation while ascending through the sediment column, the remaining Hg^0 becomes enriched in the ^{202}Hg isotope, leading to increased $\delta^{202}Hg$ values in the produced Hg(II) at higher sediment layers. While under anoxic conditions of the deep sediments, organic matter-driven dark reduction converts sediment Hg(II) into Hg°, leading to a notable negative odd-MIF.

Although quantitative data are not available at this point, we can still speculate on the importance of methane seep activities on deep-sea Hg cycling. In this study, we observed that Hg and MMHg enriched in the upper 12 cm of sediment cores in the active area with an average concentration of 97.2 ng g^{-1} and 0.21 ng g^{-1}, respectively, which is 2.4 times and 10.5 times more than those in the reference area. Given that the total active seep areas in Haima is about 350 km^2 [44], and the sediment mean bulk dry density is 1.3 g/cm^3 [45], an additional 3.15 Mg Hg and 0.01 Mg MMHg will be preserved in the active seep sediments, compared to the same area scale of the reference area. There are approximately more than 900 cold seeps that have been found globally up to date[46]. To appropriately contextualize our findings on a global scale, we have extrapolated the data from the Haima seep area to estimate the potential Hg and methylmercury (MMHg) storage across global seep systems. If we assume that other cold seeps have a comparable scale of active area with Haima, then we estimate that an additional 2835 Mg Hg and 9 Mg MMHg could be stored in cold seeps globally. According to Hayes et al.[21], the global deep-sea burial fluxes of Hg are on the order of 220 Mg Hg per year, and Zhang et al.[47]. report a global burial flux of about 9 Mg MMHg per year. Based on these figures, the total amount of additional Hg and MMHg stored in global cold seep surface sediments could correspond to about 13 year's and 1 year's worth of the global deep-sea annual burial flux for Hg and MMHg, respectively. This speculation may underestimate the influence of cold seeps on global Hg cycling, as more and more marine cold seeps will be discovered, accompanying growth in seafloor survey coverage. Moreover, while the cold seep Hg/MMHg reservoir (in Mg) is relatively small, fluxes (in Mg/y) may be important, and future work should address this. Nevertheless, our result suggests that cold seeps are an important sink of Hg and a source of MMHg in the deep ocean, which had not been previously accounted for.

Methods

Sampling

Bivalve samples and sediment cores A2, A3, A4, B1, B2, and C1 were collected in the northern part of the South China Sea (Supplementary Fig. 1), the Haima cold seep area[48] via the R/V Tansuo Yihao using the manned submersible ShenHai YongShi in 2018–2019. *G. haimaensis* collected from the active area was approximately 8 cm long, while *C. marissinica* collected from the inactive area was approximately 13 cm long. The length of the sediment push cores fell in a range of 14–30 cm. Porewater was extracted on-board immediately using a Rhizon sampler, which can effectively avoid oxidation during the extraction process. Before measurement for major ions and dissolved inorganic carbon, porewater was stored at 4 °C for one week. After pore water extraction, sediment subsamples were immediately sectioned onboard into slices of 2 cm in thickness and stored at −80 °C for geochemical and molecular analyses. The gill and tissue subsamples of the

bivalves were separated with sterile scissors onboard and stored at −80 °C for Hg analyses.

Hg, MMHg, and Hg isotope measurements

Total Hg, MMHg, and Hg isotopes in the bivalve tissues and sediments were measured at the State Key Laboratory of Environmental Geochemistry, Institute of Geochemistry, Chinese Academy of Sciences. Total Hg was measured in a total of 5 different cores. It was measured on a Direct Mercury Analyzer (DMA 80, Milestone Inc., Italy) following the US Environmental Protection Agency Method 7473[49]. The quality assurance and quality control were conducted using method blanks, sample duplicates, and certified reference materials (CRM, ERM-CC580, estuarine sediment). Method blanks were <1% of the Hg mass of the measured samples. The recoveries were 103%–105%, as assessed by ERM-CC580. The measured total Hg in ERM-CC580 was 137 ± 1.2 mg kg^{-1} (SD, $n = 3$), while the certified value is 132 ± 3 mg kg^{-1}. The relative standard deviations of sample/CRM duplicates were <5% for total Hg concentration. MMHg was measured in the two bivalve samples and three cores (A2, B1, and C1). For the analysis of MMHg, the bivalve tissue samples were digested with 25% KOH solutions at 75 ~ 80 °C in a water bath for three hours, while the sediment samples were pretreated with $CuSO_4$–HNO_3 leaching, CH_2Cl_2 extraction, and back extraction[50,51]. Then, the solution was ethylated with $NaB(C_2H_5)_4$, followed by a purge and trap with a Tenax trap, and finally analyzed by the combination of gas chromatography and cold vapor atomic fluorescence spectrometry[52]. Method blanks were 0.001 ± 0.010 ng g^{-1}. The recoveries were 93%–104% as assessed by ERM-CC580 for sediments and 104%–111% by DORM-4 for bivalve samples. The measured MMHg in ERM-CC580 was 73.9 ± 4.20 ng g^{-1} (SD, $n = 3$), while the certified value is 75.0 ± 4.00 ng g^{-1}. The measured MMHg in DORM-4 was 376 ± 14.5 ng g^{-1} (SD, $n = 3$), while the certified value is 355 ± 28.0 ng g^{-1}. The relative standard deviations of sample/CRM duplicates were <10% for MMHg concentrations.

Hg isotopes were measured in the two bivalve samples and three cores (A2, B1, and C1). For the analysis of Hg isotopes, biological tissue samples were digested in 5 mL HNO_3 at 95 °C in a water bath for 3 h, and then the digestion was oxidized by BrCl overnight, followed by hydroxylamine hydrochloride reduction before isotope determination[53]. For sediment samples, a double-stage tube furnace coupled with 40% reverse aqua regia (HNO_3/HCl = 3/1, v/v) trapping solutions were used for Hg preconcentration prior to the isotope analysis[54]. All the solutions were diluted to 0.5–1 mg L^{-1} Hg and analyzed on a Nu-Plasma II MC-ICP-MS. NIST SRM 997 Tl standard was used as an internal standard for simultaneous instrumental mass bias correction of Hg. The NIST SRM 3133 Hg standard solution was used as a bracketing standard to obtain high precision of Hg isotope analysis.

Hg isotopic results are expressed as delta (δ) values in units of per mille (‰) variation relative to the bracketed NIST-3133 Hg standard, as follows:

$$\delta^{202}Hg = [(^{202}Hg/^{198}Hg)_{sample}/(^{202}Hg/^{198}Hg)_{standard} - 1] \times 1000$$

The Hg concentration and acid matrices in the bracketing NIST-3133 solutions were matched with neighboring samples. Any Hg-isotopic value that did not follow the theoretical mass-dependent fractionation (MDF) was considered an isotopic anomaly caused by mass-independent fractionation (MIF). MIF values, reported in Δ notation (Δ^{xxx}Hg), were calculated as the difference between measured δ^{xxx}Hg and the theoretically predicted δ^{xxx}Hg value, in units of per mille (‰), as follows:

$$\Delta^{xxx}Hg = \delta^{xxx}Hg - \beta \times \delta^{202}Hg$$

where xxx = 199, 200, 201, and β is equal to 0.2520, 0.5024, and 0.7520 for ^{199}Hg, ^{200}Hg, and ^{201}Hg, respectively. NIST-3177 secondary standard solutions were diluted to 0.5–1 mg L^{-1} Hg and measured every 10 samples. Standard reference material GSS-4 (soil) was prepared and measured in the same way as the samples. Analytical uncertainty was estimated based on replicate analyses of the NIST-3177 secondary standard solution and reported as 2 SD of NIST-3177.

Sediment and pore water geochemistry

The pore water DIC concentrations and carbon isotopes (δ^{13}C-DIC) were measured at the Stable Isotope Laboratory, Third Institute of Oceanography, Ministry of Natural Resources. Samples were prepared by injecting them into evacuated septum tubes with phosphoric acid. Released CO_2 gas was then analyzed with a continuous-flow isotope ratio mass spectrometer (MAT253, Gasbench). The stable isotopic results are reported with δ values as deviations per million from the V-PDB standard. The precision based on replicate analysis was ±0.2‰ for δ^{13}C-DIC.

The sediment TOC and TN concentrations were measured on an elemental analyzer, connected to a stable isotope mass spectrometer (EA/IRMS, Elementar Vario Isotope Cube™/Isoprime 100™). Sulfate concentrations in pore water were measured by ion chromatography (ICS-1100, Thermo Inc., US).

Metagenome sequencing and analysis

DNA was extracted from the three sediment core samples (B1, B2, and C1) using PowerSoil DNA Isolation Kits (MO BIO Laboratories) according to the manufacturer's instructions. Metagenomic sequencing was performed on DNBSEQ-T1 and BGISEQ500 sequencers (MGI Tech, China).

Raw reads derived from metagenome libraries were quality-controlled by clipping off primers and adapters and filtering out artifacts and low-quality reads using the Read_QC module within the metaWRAP pipeline v1.3.2[55]. Filtered reads were individually assembled and co-assembled using MEGAHIT v1.1.3 (k list: 21, 29, 39, 59, 79, 99, 119)[56]. Each assembly was binned using the binning module within the metaWRAP pipeline v1.3.2 (–metabat2 –maxbin2 –concoct for individual assembly and co-assembly from inactive samples; –metabat2 for co-assembly from active samples). For each assembly, the three bin sets (one for co-assembly from active samples) were consolidated into a final bin set with the bin_refinement module of metaWRAP pipeline v1.3.2 (-c 50 -x 10). Finally, 865 MAGs were obtained from the 18 assemblies. They were then combined and dereplicated using dRep v 3.0.0 (-comp 50 -con 10 -sa 0.95)[57] at 95% average nucleotide identity clustering[58,59]. The completeness and contamination of each MAG were assessed using the lineage-specific workflow of CheckM v1.0.18[60]. After dereplication, a total of 487 dereplicated MAGs were obtained. Contigs in each MAG were renamed using anvi-script-reformat-fasta in anvi'o v6[61]. Each MAG was taxonomically assigned according to the Genome Taxonomy Database (GTDB) (Release R06-RS202) using GTDB-tk v1.5.0[62]. CoverM v0.6.1 "genome" (https://github.com/wwood/CoverM) was used to obtain coverage of genomes.

Functional annotations

To generate the reference gene catalog for microbial communities, genes were predicted from 18 assemblies using Prodigal v2.6.3 (-p meta). All the predicted genes were pooled (n = 12,650,024) and clustered at 95% sequence similarity and 90% alignment coverage of the shorter sequence using *cd-hit-est* option in CD-HIT v4.8.1[63]. The parameters are as follows: -c 0.95 -T 0 -M 0 -G 0 -aS 0.9 -g 1 -r 1 -d 0. This produced 6,655,350 nonredundant gene clusters, with the longest sequence of each cluster being selected for downstream analysis. To quantify gene abundance from the reference gene catalog in different metagenomes, Salmon v1.4.0[64] was used in mapping-based mode (salmon quant, --validateMappings --meta). Annotation of genes for Hg methylation (*hgcAB*), demethylation (*merB*), and reduction (*merA*) was based on published hidden Markov model (HMM) profiles (https://github.com/elizabethmcd/MEHG)[65].

For phylogenetic analysis, amino acid sequences were aligned using MAFFT v7.490 (-auto option)[66], which was further trimmed using TrimAl v1.2.59 (-gappyout option)[67]. Maximum likelihood trees were constructed using IQ-TREE v2.1.2[68], using ModelFinder to select the best model of evolution and 1000 SH-aLRT bootstraps.

Reporting summary

Further information on research design is available in the Nature Portfolio Reporting Summary linked to this article.

Data availability

Raw metagenomic sequencing data were deposited in NCBI (PRJNA739036). Large Supplementary Data, including geochemical data and metagenome statistics, were deposited in Figshare.

Received: 7 October 2023; Accepted: 30 May 2024;
Published online: 14 June 2024

References

1. Outridge, P. M., Mason, R. P., Wang, F., Guerrero, S. & Heimburger-Boavida, L. E. Updated Global and Oceanic Mercury Budgets for the United Nations Global Mercury Assessment 2018. *Environ. Sci. Technol.* **52**, 11466–11477 (2018).
2. Selin, N. E. Global biogeochemical cycling of mercury: a review. *Annu. Rev. Environ. Resour.* **34**, 43–63 (2009).
3. Lin, H. et al. Mercury methylation by metabolically versatile and cosmopolitan marine bacteria. *ISME J.* **15**, 1810–1825 (2021).
4. Villar, E., Cabrol, L. & Heimburger-Boavida, L. E. Widespread microbial mercury methylation genes in the global ocean. *Environ. Microbiol. Rep.* **12**, 277–287 (2020).
5. Liu, M. et al. Substantial accumulation of mercury in the deepest parts of the ocean and implications for the environmental mercury cycle. *Proc. Natl Acad. Sci. USA* **118**, e2102629118 (2021).
6. Lamborg, C. H. et al. A global ocean inventory of anthropogenic mercury based on water column measurements. *Nature* **512**, 65–68 (2014).
7. Zhang, Y., Jaeglé, L. & Thompson, L. Natural biogeochemical cycle of mercury in a global three-dimensional ocean tracer model. *Glob. Biogeochem. Cycles* **28**, 553–570 (2014).
8. Fitzgerald, W. F., Engstrom, D. R., Mason, R. P. & Nater, E. A. The case for atmospheric mercury contamination in remote areas. *Environ. Sci. Technol.* **32**, 1–7 (1998).
9. Beckers, F. & Rinklebe, J. Cycling of mercury in the environment: sources, fate, and human health implications: a review. *Crit. Rev. Environ. Sci. Technol.* **47**, 693–794 (2017).
10. Sun, R. et al. Methylmercury produced in upper oceans accumulates in deep Mariana Trench fauna. *Nat. Commun.* **11**, 3389 (2020).
11. Sunderland, E. M., Krabbenhoft, D. P., Moreau, J. W., Strode, S. A. & Landing, W. M. Mercury sources, distribution, and bioavailability in the North Pacific Ocean: insights from data and models. *Glob. Biogeochem. Cycles* **23**, n/a-n/a (2009).
12. Cossa, D. et al. Mercury in the Southern Ocean. *Geochim. Cosmochim. Acta* **75**, 4037–4052 (2011).
13. Blum, J. D. et al. Mercury isotopes identify near-surface marine mercury in deep-sea trench biota. *Proc. Natl Acad. Sci. USA* **117**, 29292–29298 (2020).
14. Bowman, K. L., Lamborg, C. H. & Agather, A. M. A global perspective on mercury cycling in the ocean. *Sci. Total Environ.* **710**, 136166 (2020).
15. Judd, A. G., Hovland, M., Dimitrov, L. I., Garcia Gil, S. & Jukes, V. The geological methane budget at Continental Margins and its influence on climate change. *Geofluids* **2**, 109–126 (2002).
16. Li, J., Peng, X., Bai, S., Chen, Z. & Van Nostrand, J. D. Biogeochemical processes controlling authigenic carbonate formation within the sediment column from the Okinawa Trough. *Geochim. Cosmochim. Acta* **222**, 363–382 (2018).
17. Dong, X. et al. Metabolic potential of uncultured bacteria and archaea associated with petroleum seepage in deep-sea sediments. *Nat. Commun.* **10**, 1816 (2019).
18. Dong, X. et al. Thermogenic hydrocarbon biodegradation by diverse depth-stratified microbial populations at a Scotian Basin cold seep. *Nat. Commun.* **11**, 5825 (2020).
19. Dong, X. et al. Phylogenetically and catabolically diverse diazotrophs reside in deep-sea cold seep sediments. *Nat. Commun.* **13**, 4885 (2022).
20. Vigneron, A., Cruaud, P., Aube, J., Guyoneaud, R. & Goni-Urriza, M. Transcriptomic evidence for versatile metabolic activities of mercury cycling microorganisms in brackish microbial mats. *NPJ Biofilms Microbiomes* **7**, 83 (2021).
21. Hayes, C. T. et al. Global ocean sediment composition and burial flux in the deep sea. *Glob. Biogeochem. Cycles* **35**, e2020GB006769 (2021).
22. Sanei, H. et al. High mercury accumulation in deep-ocean hadal sediments. *Sci. Rep.* **11**, 10970 (2021).
23. Yuan, J. et al. Mercury isotopes in deep-sea epibenthic biota suggest limited Hg transfer from photosynthetic to chemosynthetic food webs. *Environ. Sci. Technol.* **57**, 6550–6562 (2023).
24. Chakraborty, P., Sarkar, A., Vudamala, K., Naik, R. & Nath, B. N. Organic matter—a key factor in controlling mercury distribution in estuarine sediment. *Mar. Chem.* **173**, 302–309 (2015).
25. Heimbürger, L.-E. et al. Natural and anthropogenic trace metals in sediments of the Ligurian Sea (Northwestern Mediterranean). *Chem. Geol.* **291**, 141–151 (2012).
26. Gobeil, C., Macdonald, R. W. & Smith, J. N. Mercury Profiles in Sediments of the Arctic Ocean Basins. *Environ. Sci. Technol.* **33**, 4194–4198 (1999).
27. Gu, B. et al. Mercury reduction and complexation by natural organic matter in anoxic environments. *Proc. Natl Acad. Sci. USA* **108**, 1479–1483 (2011).
28. Dunham-Cheatham, S., Mishra, B., Myneni, S. & Fein, J. B. The effect of natural organic matter on the adsorption of mercury to bacterial cells. *Geochim. Cosmochim. Acta* **150**, 1–10 (2015).
29. Gilmour, C. C., Bullock, A. L., McBurney, A., Podar, M. & Elias, D. A. Robust mercury methylation across diverse methanogenic archaea. *mBio* **9**, e02403–e02417 (2018).
30. Ma, M., Du, H. & Wang, D. Mercury methylation by anaerobic microorganisms: a review. *Crit. Rev. Environ. Sci. Technol.* **49**, 1893–1936 (2019).
31. Fu, W. et al. Production of ancient dissolved organic carbon in arctic ocean sediment: a pathway of carbon cycling in the extreme environment. *Geophys. Res. Lett.* **47**, e2020GL087119 (2020).
32. Gfeller, L., Weber, A., Worms, I., Slaveykova, V. I. & Mestrot, A. Mercury mobility, colloid formation and methylation in a polluted Fluvisol as affected by manure application and flooding–draining cycle. *Biogeosciences* **18**, 3445–3465 (2021).
33. Blum, J. D., Sherman, L. S. & Johnson, M. W. Mercury isotopes in earth and environmental sciences. *Annu. Rev. Earth Planet. Sci.* **42**, 249–269 (2014).
34. Sun, R. et al. Modelling the mercury stable isotope distribution of Earth surface reservoirs: Implications for global Hg cycling. *Geochim. Cosmochim. Acta* **246**, 156–173 (2019).
35. Bergquist, B. A. & Blum, J. D. Mass-dependent and -independent fractionation of hg isotopes by photoreduction in aquatic systems. *Science* **318**, 417–420 (2007).
36. Jiskra, M. et al. Mercury stable isotopes constrain atmospheric sources to the ocean. *Nature* **597**, 678–682 (2021).
37. Zheng, W. et al. Mercury stable isotope fractionation during abiotic dark oxidation in the presence of thiols and natural organic matter. *Environ. Sci. Technol.* **53**, 1853–1862 (2019).
38. Zheng, W. & Hintelmann, H. Nuclear field shift effect in isotope fractionation of mercury during abiotic reduction in the absence of light. *J. Phys. Chem. A* **114**, 4238–4245 (2010).
39. Jiskra, M., Sonke, J. E., Agnan, Y., Helmig, D. & Obrist, D. Insights from mercury stable isotopes on terrestrial–atmosphere exchange of Hg(0) in the Arctic tundra. *Biogeosciences* **16**, 4051–4064 (2019).
40. Guédron, S. et al. Mercury isotopic fractionation during pedogenesis in a tropical forest soil catena (French Guiana): deciphering the impact of historical gold mining. *Environ. Sci. Technol.* **52**, 11573–11582 (2018).

41. Podar, M. et al. Global prevalence and distribution of genes andmicroorganisms involved in mercury methylation. *Sci. Adv.* **1**, e1500675 (2015).
42. Orsi, W. D. Ecology and evolution of seafloor and subseafloor microbial communities. *Nat. Rev. Microbiol* **16**, 671–683 (2018).
43. Krout, I. N., Scrimale, T., Vorojeikina, D., Boyd, E. S. & Rand, M. D. Organomercurial lyase (MerB)-mediated demethylation decreases bacterial methylmercury resistance in the absence of mercuric reductase (MerA). *Appl. Environ. Microbiol.* **88**, e0001022 (2022).
44. Yao, G. et al. Community characteristics and genetic diversity of macrobenthos in haima cold seep. *Front. Mar. Sci.* **9**, 920327 (2022).
45. Hou, Z. et al. Seafloor sediment study from south china sea: acoustic & physical property relationship. *Remote Sens.* **7**, 11570–11585 (2015).
46. Feng, J. C. et al. Tracing the century-long evolution of microplastics deposition in a cold seep. *Adv. Sci. (Weinh.)* **10**, e2206120 (2023).
47. Zhang, Y., Soerensen, A. L., Schartup, A. T. & Sunderland, E. M. A global model for methylmercury formation and uptake at the base of marine food webs. *Glob. Biogeochem. Cycles* **34**, e2019GB006348 (2020).
48. Liang, Q. et al. Authigenic carbonates from newly discovered active cold seeps on the northwestern slope of the South China Sea: constraints on fluid sources, formation environments, and seepage dynamics. *Deep Sea Res. Part I* **124**, 31–41 (2017).
49. USEPA, Method 7473: Mercury in solids and solutions by thermal decomposition, amalgamation, and atomic absorption spectrophotometry (2007).
50. Yan, H. Y., Feng, X. B., Liang, L., Shang, L. H. & Jiang, H. M. Determination of methyl mercury in fish using GC-CVAFS. *J. Instrum. Anal.* **24**, 78–80 (2005).
51. Liang, L., Horvat, M., Cernichiari, E., Gelein, B. & Balogh, S. Simple solvent extraction technique for elimination of matrix interferences in the determination of methylmercury in environmental and biological samples by ethylation-gas chromatography-cold vapor atomic fluorescence spectrometry. *Talanta* **43**, 1883–1888 (1996).
52. USEPA, Method 1630, methyl mercury in water by distillation, aqueous ethylation, purge and trap, and CVAFS. (US Environmental Protection Agency, Washington, DC, 1998).
53. USEPA, Method 1631, Revision E: mercury in water by oxidation, purge and trap, and cold vapor atomic fluorescence spectrometry. (US Environmental Protection Agency Washington, DC, 2002).
54. Yu, B. et al. Isotopic composition of atmospheric mercury in China: new evidence for sources and transformation processes in air and in vegetation. *Environ. Sci. Technol.* **50**, 9262–9269 (2016).
55. Uritskiy, G. V., DiRuggiero, J. & Taylor, J. MetaWRAP—a flexible pipeline for genome-resolved metagenomic data analysis. *Microbiome* **6**, 158 (2018).
56. Li, D. et al. MEGAHIT v1.0: a fast and scalable metagenome assembler driven by advanced methodologies and community practices. *Methods* **102**, 3–11 (2016).
57. Olm, M. R., Brown, C. T., Brooks, B. & Banfield, J. F. dRep: a tool for fast and accurate genomic comparisons that enables improved genome recovery from metagenomes through de-replication. *ISME J.* **11**, 2864–2868 (2017).
58. Jain, C., Rodriguez, R. L., Phillippy, A. M., Konstantinidis, K. T. & Aluru, S. High throughput ANI analysis of 90K prokaryotic genomes reveals clear species boundaries. *Nat. Commun.* **9**, 5114 (2018).
59. Olm, M. R. et al. Consistent metagenome-derived metrics verify and delineate bacterial species boundaries. *mSystems* **5**, e00731-19 (2020).
60. Parks, D. H., Imelfort, M., Skennerton, C. T., Hugenholtz, P. & Tyson, G. W. CheckM: assessing the quality of microbial genomes recovered from isolates, single cells, and metagenomes. *Genome Res.* **25**, 1043–1055 (2015).
61. Eren, A. M. et al. Anvi'o: an advanced analysis and visualization platform for 'omics data. *PeerJ* **3**, e1319 (2015).
62. Chaumeil, P. A., Mussig, A. J., Hugenholtz, P. & Parks, D. H. GTDB-Tk: a toolkit to classify genomes with the Genome Taxonomy Database. *Bioinformatics* **36**, 1925–1927 (2019).
63. Fu, L., Niu, B., Zhu, Z., Wu, S. & Li, W. CD-HIT: accelerated for clustering the next-generation sequencing data. *Bioinformatics* **28**, 3150–3152 (2012).
64. Patro, R., Duggal, G., Love, M. I., Irizarry, R. A. & Kingsford, C. Salmon provides fast and bias-aware quantification of transcript expression. *Nat. Methods* **14**, 417–419 (2017).
65. McDaniel, E. A. et al. Expanded phylogenetic diversity and metabolic flexibility of mercury-methylating microorganisms. *mSystems* **5**, e00299-20 (2020).
66. Katoh, K. & Standley, D. M. A simple method to control over-alignment in the MAFFT multiple sequence alignment program. *Bioinformatics* **32**, 1933–1942 (2016).
67. Capella-Gutierrez, S., Silla-Martinez, J. M. & Gabaldon, T. trimAl: a tool for automated alignment trimming in large-scale phylogenetic analyses. *Bioinformatics* **25**, 1972–1973 (2009).
68. Nguyen, L. T., Schmidt, H. A., von Haeseler, A. & Minh, B. Q. IQ-TREE: a fast and effective stochastic algorithm for estimating maximum-likelihood phylogenies. *Mol. Biol. Evol.* **32**, 268–274 (2015).

Acknowledgements

The authors wish to thank all the participants on the manned submersible ShenHaiYongShi and the R/V TANSUOYIHAO during the South China Sea Expedition in 2018-2019. This work was funded by the National Key Research and Development Program of China (Grant No. 2022YFC2805500), the National Natural Science Foundation of China (Grant Nos. 42176072, 41876050 and 41921004), the Opening Fund of the State Key Laboratory of Environmental Geochemistry (SKLEG20202020210), the Hainan Province Science and Technology Talents Innovation Project (KJRC2023C14), the Guizhou Provincial 2019 Science and Technology Subsidies (No. GZ2019SIG), and the French National Funding Agency (HydrOThermal Mercury ANR-21-CE34-0026). We declare that the collection of samples conducted in this study does not require any specific permissions or permits.

Author contributions

J.L. and X.P. designed this research. X.D., Y.T., C.Z., and S.L. performed microbial analysis and analyzed data. L.S., W.Z., Y.T., W.Y., and X.F. performed the Hg geochemical analysis and analyzed data. J.L., X.D., L.S., Y.T., Y.Y., F.W., and L.E.H.B. wrote the paper. J.L. and Y.T. participated in cruises and collected samples. All authors discussed the results.

Competing interests

The authors declare no competing interests.

Additional information

Supplementary information The online version contains supplementary material available at https://doi.org/10.1038/s43247-024-01484-7.

Correspondence and requests for materials should be addressed to Lihai Shang or Xiaotong Peng.

Peer review information *Communications Earth & Environment* thanks the anonymous reviewers for their contribution to the peer review of this work. Primary Handling Editors: Mojtaba Fakhraee, Clare Davis, and Alice Drinkwater. A peer review file is available.